We are IntechOpen,
the world's leading publisher of
Open Access books
Built by scientists, for scientists

6,900
Open access books available

186,000
International authors and editors

200M
Downloads

Our authors are among the

154
Countries delivered to

TOP 1%
most cited scientists

12.2%
Contributors from top 500 universities

CLARIVATE ANALYTICS
BOOK CITATION INDEX
INDEXED

WEB OF SCIENCE™

Selection of our books indexed in the Book Citation Index
in Web of Science™ Core Collection (BKCI)

Interested in publishing with us?
Contact book.department@intechopen.com

Nanocomposites for Organic Light Emiting Diodes

Nguyen Nang Dinh
University of Engineering and Technology, Vietnam National University Hanoi
Vietnam

1. Introduction

Recently, both the theoretical and experimental researches on conducting polymers and polymer-based devices have strongly been increasing (Salafsky, 1999, Huynh, 2002, Petrella et al., 2004, Burlakov et al., 2005), due to their potential application in optoelectronics, organic light emiting diode (OLED) displays, solar flexible cells, etc. Similar to inorganic semiconductors, from the point of energy bandgap, conducting polymers also have a bandgap – the gap between the highest occupied molecular orbital (HOMO) and the lowest unoccupied molecular orbital (LUMO). When sufficient energy is applied to a conducting polymer (or a semiconductor), it becomes conducting excitation of electrons from the HOMO level (valence band) into the LUMO level (conduction band). This excitation process leaves holes in the valence band, and thus creates "electron-hole-pairs" (EHPs). When these EHPs are in intimate contact (i.e., the electrons and holes have not dissociated) they are termed "excitons". In presence of an external electric field, the electron and the hole will migrate (in opposite directions) in the conduction and valence bands, respectively (Figure 1).
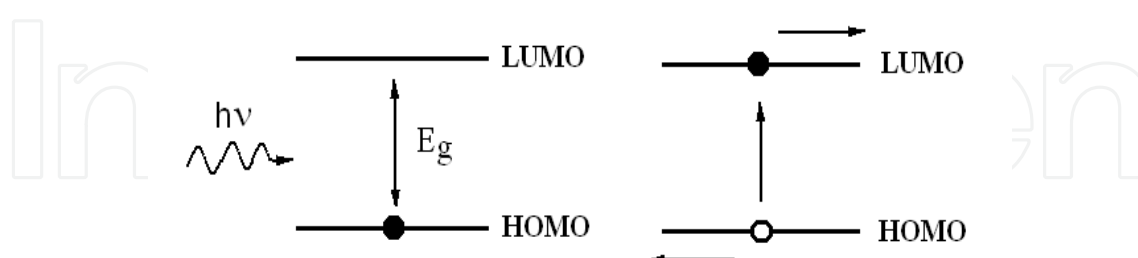

Fig. 1. Formation of "electron-hole pair" induced by an excitation from an external energy source (Klabunde, 2001)

On the other hand, inorganic semiconductors when reduce to the nanometer regime possess characteristics between the classic bulk and molecular descreptions, exhibiting properties of quantum confinement. These materials are reflected to as nanoparticles (or nanocrystals), or

"quantum dot". Thus, adding metallic, semiconducting, and dielectric nanocrystals into polymer matrices enables enhance the efficiency and service duration of the devices. The inorganic additives usually have nanoparticle form. Inorganic nanoparticles can substantially influence the mechanical, electrical, and optical (including nonlinear optical as well as photoluminescent, electroluminescent, and photoconductive) properties of the polymer in which they are embedded. The influence of nanocrystalline oxides on the properties of conducting polymers has been investigated by many scientists in the world. A very rich publication has been issued regarding the nanostructured composites and nano hybrid layers or heterojunctions which can be applied for different practical purposes. Among these applications one can divide two scopes, those concern to interaction between electrons and photons such as OLED (electricity generates light) and solar cells (light generates electricity).

In this chapter there are presented two types of the nanocomposite materials: the first one is the nanostructured composite with a structure of nanoparticles embedded in polymers, abbreviated to NIP, the second one is the nanocomposite with a structure of polymers deposited on nanoporous thin films, called as PON.

2. NIP nanocomposite

2.1 The role of Ti oxide nanoparticles in NIP

It is known that a basic requirement for a photovoltaic material is to generate free charge carriers produced by photoexcitation (Petrella et al., 2004, Burlakov et al., 2005). Subsequently, these carriers are transported through the device to the electrodes without recombining with oppositely charged carriers. Due to the low dielectric constant of organic materials, the dominant photogenerated species in most conjugated polymer is a neutral bound electron–hole pair (exciton). These neutral excitons can be dissociated from Coulomb attraction by offering an energetically favorable pathway for the electron from polymer (donor) to transfer to electron-accepting specie (acceptor). Charge separation in the polymer is often enhanced by inclusion of a high electron affinity substance such as C_{60} (Salafsky, 1999) organic dyes (Huynh et al., 2002, Ma et al., 2005), or nanocrystals (Burlakov et al., 2005). Nanocrystals are considered more attractive in photovoltaic applications due to their large surface-to-bulk ratio, giving an extension of interfacial area for electron transfer, and higher stability. The charge separation process must be fast compared to radiative or non-radiative decays of the singlet exciton, leading to the quench of the photoluminescence (PL) intensities. In addition, electron transport in the polymer/nanoparticle hybrid is usually limited by poorly formed conduction path. Thus, one-dimensional semiconductor nanorods are preferable over nanoparticles for offering direct pathways for electric conduction. It has been demonstrated that the solar cell based on the CdSe nanorods/poly(3-hexylthiophene)(P3HT) hybrid material exhibits a better power conversion efficiency than its CdSe nanoparticle counterpart. The environmental friendly and low-cost TiO_2 nanocrystal is another promising material in hybrid polymer/nanocrystal solar cell applications (Haugeneder, 1999, Dittmer et al., 2000).

The influence of nanooxides on the photoelectric properties of nanocomposites is explained with regard to the fact that TiO_2 particles usually form a type-II heterojunction with a polymer matrix, which essentially results in the separation of nonequilibrium electrons and holes. Embedding SiO_2 particles results in stabilization of the nanocomposite properties and

an increase in the lifetime of polymer-based electroluminescent devices. It is usually assumed that embedding semiconducting or dielectric nanocrystals creates additional potential wells and/or barriers for carriers and does not influence the energy spectrum of the polymer itself, except for a possible implicit influence through a change of the polymer conjugated length. However, it is also known that, in a conducting polymer with very low carrier mobility, the energy of carriers is determined to a considerable degree by the polarization of the material, which influences the position of the HOMO and LUMO levels as well as the exciton energy. The influence can be considerable, and can result in energy shifts of the order of 1 eV for free (unbound) electrons and holes in a polymer. In a uniform polymer medium this component of energy is determined by the molecular structure of the polymer and the fabrication technology. In nonuniform media, such as polymer–nanocrystal mixtures, the picture may change. In that case the polarization energy component may additionally depend on the relative position of carriers and inorganic inclusions.

Results in time-resolved PL measurements were reported (Dittmer et al., 2000). It is seen that time evolution of PL intensity of poly[2-methoxy-5-(2'-ethyl-hexyloxy)-1,4-phenylene vinylene] (MEH–PPV) on quartz shows mono-exponential decrease due to natural decay of excitons with a characteristic time constant 300 ps. PL intensity of MEH–PPV on TiO_2 decreases at initial time much quicker than that for MEH–PPV on quartz due to exciton quenching at the interface with TiO_2 substrate (Figure 2).
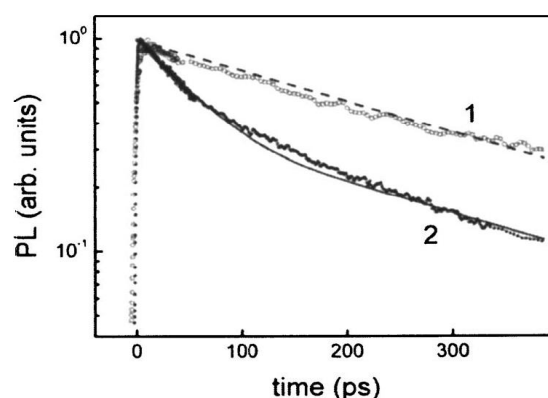

Fig. 2. PL intensity as a function of time in logarithmic scale. The symbols are experimental data for MEH-PPV film deposited on quartz (1) and TiO_2 (2) substrates, respectively. The dashed curve corresponds to monoexponential decay enabling determination of exciton life-time τ. The solid curve is theoretically calculated (Burlakov, et al., 2005)

TiO_2 nanocrystals – MEH-PPV composite thin films have also been studied as photoactive material (Petrella et al., 2004). It has been shown that MEH-PPV luminescence quenching is strongly dependent on the nature of nanostructral particles embedded in polymer matrix. Fluorescence quenching is much higher with rod titanium dioxide. In principle, rod particles can be expected to exhibit higher photoactivity with respect to spherical particles. In fact, when compared with the dot-like shape, rod-like geometry is advantageous for a more efficient packing of the inorganic units, owing to both a higher contact area and more intensive van der Waals forces. Actually, the higher quenching of the polymer fluorescence observed in presence of titania nanoparticles (Figure 3) proves that transfer of the photogenerated electrons to TiO_2 is more efficient for rods.
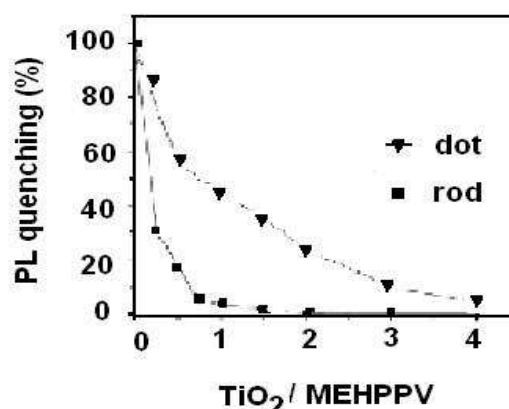
Fig. 3. MEH-PPV luminescence quenching vs. TiO$_2$/polymer volume ratio at λ = 480 nm (Petrella et al., 2004)

Chronoamperometric measurements have been performed on films of MEH-PPV, nanocrystalline TiO$_2$ and their blends. Thin films were deposited onto ITO from CHCl$_3$ solutions by spin-coating and immersed into an acetonitrile solution of tetrabutylammonium-perchlorate. As the authors showed, the light absorption and electron-hole pair photogeneration occur exclusively in MEH-PPV. The electron is then injected into the conduction band of the inorganic material, while the hole is transferred to the interface with electrolyte solution. Figure 4 indicates a higher photoactivity in blends when compared to the single components; the anodic photocurrents are higher with respect to the currents measured for MEH-PPV thin films, and are very reproducible. High film photostability was observed under longterm operative conditions.
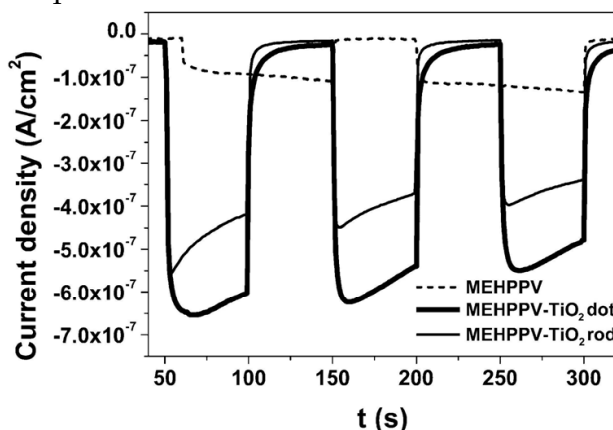

Fig. 4. Chronoamperometric measurements of MEH-PPV (...., blends of MEH-PPV TiO$_2$ dots (—) and MEH-PPV TiO$_2$ rods (thin solid line) in a photoelectrochemical cell. Ag/AgCl is chosen as reference electrode, while ITO and platinum as working and counter-electrode, respectively. A halogen lamp is used. The films were deposited onto ITO and immersed into acetonitrile solution of tetrabutyl-ammonium-perchlorate 0.1 M (Petrella et al., 2004)

From the obtained results it is known that the deposited composites film showed a higher photoactivity when compared to the single components due to the availability of numerous interfaces for enhanced charge transfer at the hetero-junction. Effective transport of excitons in conjugated polymers is extremely important for performances of organic light emitting

diodes and of plastic excitonic solar cells. A crucial step in the photovoltaic process, for instance, is the conversion of photogenerated excitons into charge carriers at the polymer-inorganic interfaces. High quantum yield of charge carriers could be achieved if the excitons would travel far enough from their generation points to appropriate interfaces where they can dissociate, injecting electrons into the electrode. The holes remaining in the polymer diffuse to the opposite electrode, completing charge separation. Only a fraction of the photogenerated excitons reach relevant interfaces while many of them decay by emitting light or exciting vibrations of the polymer molecules.

Besides, a limited lifetime, the length scale of the exciton migration is restricted by the spatial dependence of the exciton energy - i.e., inhomogeneous broadening of exciton energy level. A conjugated polymer chain, for example, can be thought of as series of molecular segments linked with each other at topological faults. Each segment has certain LUMO and HOMO levels depending in part on its conjugation length. While migrating, excitons on average lose their energy by predominantly hopping to lower-energy sites.

Therefore the migration of excitons slows down when they reach the low-energy sites where they find fewer sites with lower energy in its neighborhood. Due to such dispersive migration, the exciton diffusion cannot be described using a constant diffusion coefficient, but a time-dependent one.

Photoluminescence efficiency was observed as a function of the content of nanocrystalline TiO_2 (nc-TiO_2) embedded in PPV, as demonstrated in figure 5 (Salafsky, 1999).
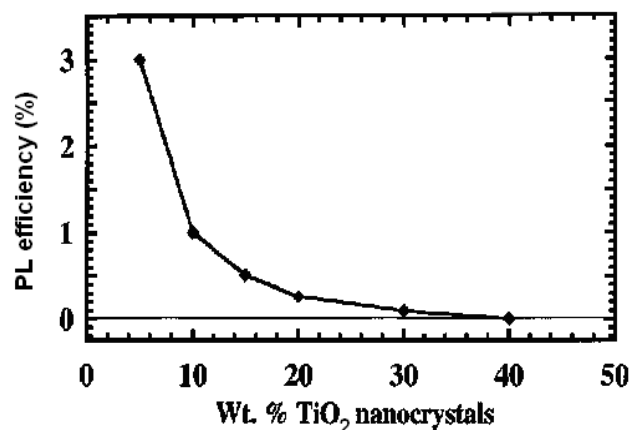

Fig. 5. Absolute photoluminescence (PL) efficiency of PPV:TiO_2 composites as a function of wt% TiO_2 nanocrystals (Salafsky, 1999)

The PL efficiency for PPV alone was measured to be 20%. This proves the PPV luminescence quenching. From point of review of photoactive materials, such a composite as PPV+nc-TiO_2 can be used for excitonic solar cells. The mechanism of the PPV luminescence quenching effect has been elucidated by energy diagram of polymer/oxide junctions (Figure 6).

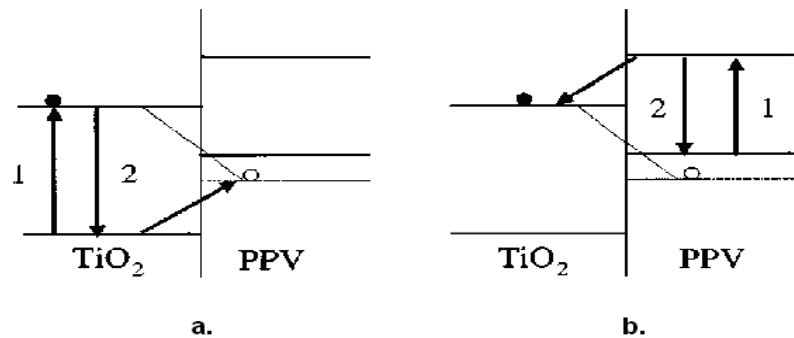a.   b.

Fig. 6. Schematic diagram of the various excitation, charge transfer, and decay pathways available in a conjugated polymer nanocrystal composite (Salafsky, 1999)

The filled circles indicate electrons, and the open circles represent holes. Process 1 indicates photoexcitation; process 2 indicates decay of the electronic excited state; the dark slanting lines with arrows indicate a hole or electron transfer process (left and right sides, respectively); and the thin lines connecting the conduction band of TiO_2 with the hole level in PPV indicate an interfacial recombination process. The state levels are depicted as in this figure, with the holes placed at slightly lower energy than the polymer LUMO.

Absorbed photon-to-conducting-electron conversion efficiency (APCE) of solar devices based on the conjugated polymer-TiO_2 composite was obtained (Salafsky, 1999, Burlakov et al., 2005). It shows that the APCE is as a function of incident photon energy obtained. The quantum efficiency (QE) of light absorption, a fraction of photons absorbed within 50-nm-thick MEH-PPV with respect to the incident photons onto a device is also plotted which shows the photo-harvesting ability of the device (Figure 7).
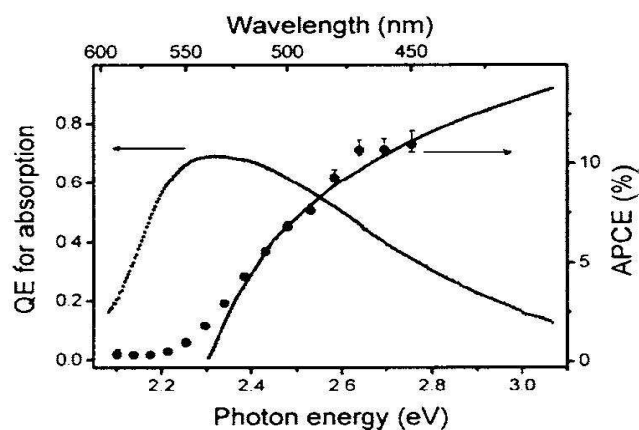

Fig. 7. Comparison of APCE curves obtained experimentally (solid circles) and theoretically (solid line) for 50-nm-thick MEH-PPV (Burlakov et al., 2005)

In a recent work (Lin et al., 2006), the authors have reported morphology and photoluminescent properties of MEH-PPV+nc-TiO_2 composites. The last is strongly dependent the excitation energy of photons. The samples were prepared with a large content of TiO_2, such as from 40 to 80 wt% of TiO_2 nanorods. The PL curves showed that the pristine MEH-PPV exhibits a broad absorption spectrum peaked at about 490 nm and TiO_2 nanorods have an absorption edge at about 350 nm. Due to the nature of indirect

semiconductor of TiO_2 nanorods, absorption and emission probabilities of indirect transition in pristine TiO_2 are much lower than for direct transitions. The inset shows the luminescence spectrum of TiO_2 nanorods excited at 280 nm. The broad emission band is mainly attributed to radiative recombination between electrons in the shallow trap states below the conduction band, the relative natural radiative lifetime resulted from oxygen vacancies and surface states, and holes in the valence band. Similar luminescence features of colloidal TiO_2 nanocrystals have been investigated previously (Ravirajan et al., 2005). For the excitation wavelengths in the range of 400-550 nm where only polymer is excited, the fluorescence intensities are further quenching, indicating that more efficient charge separation takes place with increasing TiO_2-nanorod content. In contrast, the intensities of fluorescence from polymer increase instead for the excitation wavelengths shorter than 350 nm. Due to the large absorption coefficient for TiO_2 nanorods at wavelengths less than 350 nm, the non-radiative Förster resonant energy transfer from TiO_2 nanorods to polymer may be responsible for the enhancement of fluorescence intensities. Enhancement in PL intensities in polymer suggests that absorption by TiO_2 nanorods leads to emission in the MEH-PPV by the non-radiative Förster resonant energy transfer (FRET) (Heliotis et al., 2006).

Cater et al have shown that the incorporation of nanoparticles inside an electroluminescent MEH–PPV thin film results in order of magnitude increases in current and luminance output (Figure 8). The nanoparticles appear to modify the device structures sufficiently to enable more efficient charge injection and transport as well as inhibiting the formation of current filaments and shorts through the polymer thin film. The composite nanoparticle/MEH–PPV films result in exceptionally bright and power efficient OLEDs (Cater et al., 1997). However, improvements are still needed in the device lifetime and homogeneity of the light output for these materials to be commercially viable.
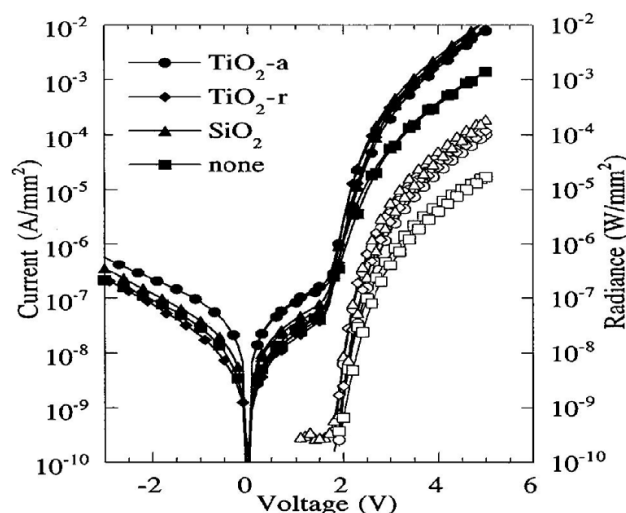

Fig. 8. Current–voltage and radiance–voltage curves for 1:1 TiO_2 (anatase)/MEH–PPV(circles), 1:1 TiO_2 (rutile)/MEH–PPV (diamonds), 1:1 SiO2/MEH–PPV (triangles), and for MEH–PPV film with no nanoparticles (squares). Close symbols are for current. Open symbols are for radiance. $1W/mm^2 = 7.3 \times 10^7$ cds/m^2 (Carter et al., 1997)

2.2 NIP composites for OLED
Polymer-based electroluminescent materials are very prospective for many applications, for instance, OLEDs are now commercialized in display fields. The efficient device operation

requires optimization of three factors: (i) equalization of injection rates of positive (hole) and negative (electron) charge carriers (ii) recombination of the charge carriers to form singlet excitons and (iii) radiative decay of the excitons. Of the two carriers, holes have the lower mobility in general and may limit the current conduction process. By adding a hole transport layer (HTL) to the three-layer device one can expect equalization of injection rates of holes and electrons, to obtain consequently a higher electroluminescent efficiency of OLED. However, both the efficiency and the lifetime of OLEDs are still lower in comparison with those of inorganic LED. To improve these parameters one can expect using nanostructured polymeric/inorganic composites, instead of standard polymers for the emitting layer.

2.2.1 NIP films for hole transport layer

To prepare a NIP of polypropylene carbazone (PVK) and CdSe quantum dots (QD), a solution of PVK was made by dissolving PVK and in pure chloroform, then CdSe-QDs were added to this solution, stirred by ultrasonic bath. The solution then was spin-coated onto both glass and tin indium oxide (ITO) substrates with spin rates ranging from 1200 rpm to 2000 rpm for 1 to 2 min (Dinh et al., 2003). Under an excitation of short wavelength laser, the intensity of the PVK-NIP much increased, as seen in figure 9. Replacing CdSe-QDs by nc-TiO$_2$ the feature of the PL-enhancement is the same. Although the PVK-NIP can be used as HTL in OLED, polyethylenedioxythiophene (PEDOT) seemed to be much better candidat for the hole transoport, because it has a high transmission in the visible region, a good thermal stability and a high conductivity (Quyang et al., 2004; Tehrani et al., 2007). To enhance the interface contact between ITO and PEDOT, TiO$_2$ nanoparticles were embedded into PEDOT (Dinh et al., 2009)
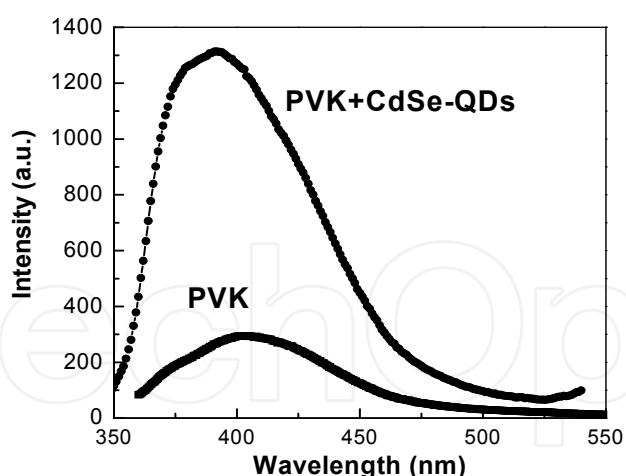

Fig. 9. Photoluminescence spetra of PVK and PVK+CdSe nanocomposite under a large photon energy excitation

Figure. 10 shows the atom force microscope (AFM) of a PEDOT composite with a percentage of 20 wt. % TiO$_2$ nanoparticles (about 5 nm in size). With such a high resolution of the AFM one can see a distribution of nanoparticles in the polymer due to the spin-coating process. For the pure polymeric PEDOT, the surface exhibits smoothness comparable to the one of the area surrounding the nanoparticles. The TiO$_2$ nanoparticles

contributed to the roughness of the composite surface and created numerous TiO_2/ PEDOT boundaries in the composite film.

Transmittance spectra respectively for a pure PEDOT and a nanocomposite films are plotted in Figure 11. From this figure one can see that nanoparticles of TiO_2 made the polymer film more absorbing in the violet range while making it more transparent in the near infrared range. At the range of the emission light of MEH-PPV, namely from 540 nm to 600 nm, the two samples have about a same transmittance of 82%. This transmittance is a bit lower, but still comparable to the transmittance of the ITO anode. Since PEDOT has a good conductivity, the electrical conductivity of this conducting polymer blend reaching up to 80 S/cm (Quyang et al., 2005), in the infrared wavelength range it reflects the IR light better resulting in a decrease in the transmittance. The presence of TiO_2 nanoparticles in PEDOT results in a cleavage of the polymer conjugation pathway, consequently leading to a decrease in film conductivity. This is why in the IR range the PEDOT composite has a higher transmittance than that of a pure PEDOT. However, this small decrease in conductivity does not affect much the performance of a OLED that uses the composite as a hole transport layer.
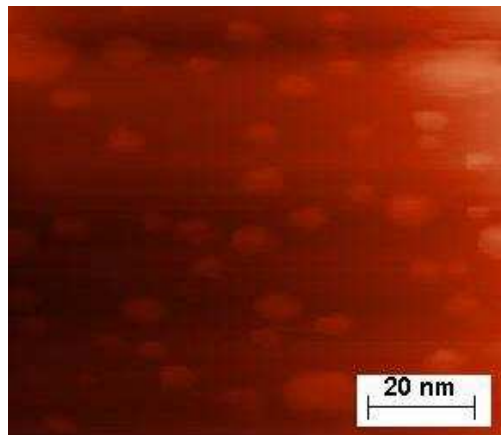

Fig. 10. AFM of a PEDOT+nc-TiO_2 composite film with embedding of 20 wt.% TiO_2 nanoparticles
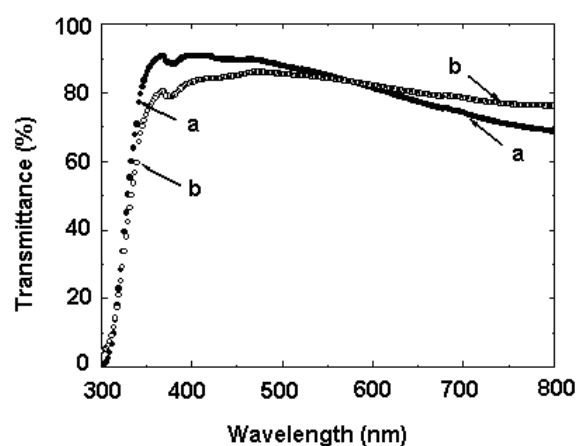

Fig. 11. Transmittance spectra of PEDOT (curve "a") and PEDOT composite films (curve "b")

2.2.2 NIP films for emitting layer

To deposit MEH-NIP composite layers, MEH-PPV solution was prepared by dissolving MEH-PPV powder in xylene with a ratio of 10 mg of MEH-PPV in 1 ml of xylene. Then,

TiO2 nanoparticles were embedded in these solutions according to a weight ratio TiO2/MEH-PPV of 0.15 (namely 15 wt. %), further referred to as MEHPPV+TiO$_2$. The last deposit was used as the emitter layer (EL). To obtain a homogenous dispersion of TiO$_2$ in polymer, the solutions were mixed for 8 hours by using magnetic stirring. These liquid composites were then used for spin-coating and casting. The conditions for spin-coating are as follows: a delay time of 120 s, a rest time of 30 s, a spin speed of 1500 rpm, an acceleration of 500 rpm and finally a drying time of 2 min. The films used for PL characterization were deposited by casting onto KBr tablets having a diameter of 10 mm, using 50 μl of the MEH-PPV solution. To dry the films, the samples were put in a flow of dried gaseous nitrogen for 12 hours (Dinh et al., 2009).

Surfaces of MEH-PPV+TiO$_2$ nanocomposite samples were examined by SEM. Figure 12 shows SEM images of a composite sample with embedding of 15 wt.% nanocrystalline titanium oxide particles (about 5 nm in size). The surface of this sample appears much smoother than the one of composites with a larger percentage of TiO$_2$ particles or with larger size TiO$_2$ particles. The influence of the heat treatment on the morphology of the films was weak, i.e. no noticeable differences in the surface were observed in samples annealed at 120°C, 150°C or 180°C in the same vacuum. But the most suitable heating temperature for other properties such as the current-voltage (I-V) characteristics and the PL spectra was found to be 150 $^{\circ}$C. In the sample considered, the distribution of TiO$_2$ nanoparticles is mostly uniform, except for a few bright points indicating the presence of nanoparticle clusters.
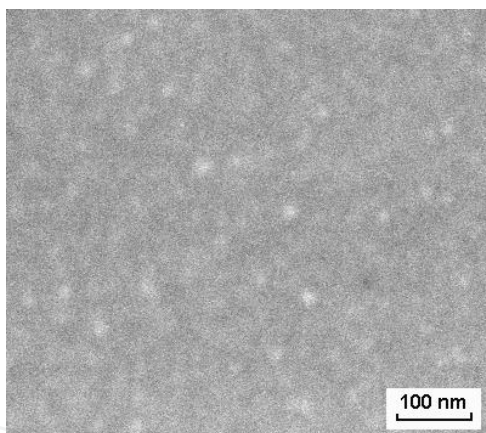

Fig. 12. SEM of a MEH+PPV-TiO$_2$ annealed in vacuum at 150 $^{\circ}$C

The results of PL measurements the MEHPPV+TiO$_2$ nanocomposite excited at a short wavelength (325 nm) and at a standard one (470 nm) are presented. Figure 13 shows plots of the photoluminescence spectra measured on a pure MEH-PPV and a composite sample, using the FL3-2 spectrophotometer with an He-Ne laser as an excitation source (λ = 325 nm). With such a short wavelength excitation both the polymer and the composite emitted only one broad peak of wavelengths. From this figure, it is seen that the photoemission of the composite film exhibits much higher luminescence intensity than that of the pure MEH-PPV. A blue shift from 580.5 nm to 550.3 nm was observed for the PL peak. This result is consistent with currently obtained result on polymeric nanocomposites (Yang et al., 2005), where the blue shift was explained by the reduction of the chain length of polymer, when nanoparticles were embedded in this latter. Although PL enhancement has been rarely

mentioned, one can suggest that the increase in the PL intensity for such a composite film can be explained by the large absorption coefficient for TiO_2 particles. Indeed, this phenomenon would be attributed to the non-radiative FRET from TiO_2 nanoparticles to polymer with excitation of wavelength less than 350 nm.
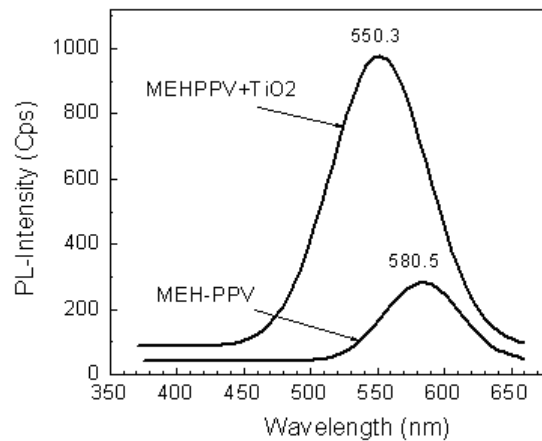

Fig. 13. PL spectra of MEH-PPV+nc-TiO_2. Excitation beam with λ = 325 nm

In figure 14 the PL spectra for the MEH-PPV and the composite films with excitation wavelength of 470 nm are plotted. In this case, the MEH-PPV luminescence quenching was observed. For both samples, the photoemission has two broad peaks respectively at 580.5 nm and 618.3 nm. The peak observed at 580.5 nm is larger than the one at 618.3 nm, similarly to the electroluminescence spectra plotted in the work of Carter et al (1997). As seen (Petrella et al., 2004) for a composite, in the presence of rod-like TiO2 nanocrystals, PPV quenching of fluorescence is significantly high. This phenomenon was explained by the transfer of the photogenerated electrons to the TiO_2. It is known (Yang et al., 2005) that the fluorescence quenching of MEH-PPV results in charge-separation at interfaces of TiO_2/MEH-PPV, consequently reducing the barrier height at those interfaces.
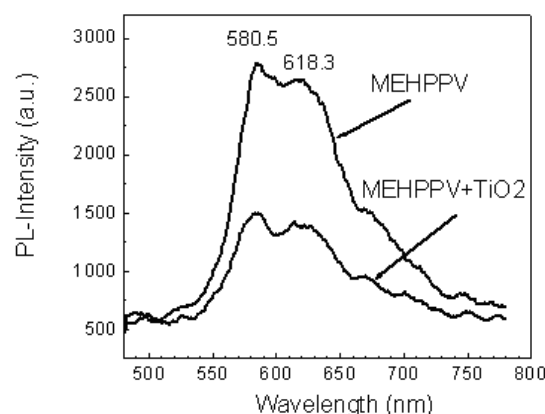

Fig.14. PL spectra of MEH-PPV+nc-TiO2. Excitation beam with λ = 470 nm

The effect of nanoparticles in composite films used for both the emitting layer (EL) and HTL in OLEDs was revealed by measuring the I-V characteristics of the devices made from different layers, such as a single pure EL diode (ITO/MEH-PPV/Al, abbreviated as SMED), a double pure polymer diode (ITO/PEDOT/MEH-PPV/Al or PPMD), a double polymeric

composite layer diode, where a MEH-PPV+TiO2 composite was used as a EL and a PEDOT-composite film was used as a HTL (ITO/PEDOT+TiO$_2$/MEH-PPV+TiO$_2$/Al or PMCD), and a multilayer OLED, where a super thin LiF layer as ETL was added (ITO/PEDOT+TiO$_2$/MEH-PPV+TiO$_2$/LiF/Al or MMCD). A 10 nm-thick LiF layer used for the SCL was e-beam deposited onto the MEH-PPV+TiO$_2$; it was then covered by an Al coating prepared by evaporation. A detailed characterization of the SCL was however not carried out here, except for a comparison of the I-V characteristics (see figure 15). From this figure one can notice the following:

(i)   The turn-on voltages for the diodes SMED, PPMD, PMCD to MMCD are found to be 3.4 V, 2.6V, 2.2 V and 1.7 V, respectively. For the full multilayer diode (MMCD), not only the turn-on voltage but also the reverse current is the smallest. This indicates the equalization of injection rates of holes and electrons due to both the HTL and the SCL which were added to the OLED.

(ii)   A pure PEDOT used as HTL favors the hole injection from ITO into the organic layer deposited on the HTL, resulting in an enhancement of the I-V characteristics. Thus the turn-on voltage decreased from 3.4 V to 2.6 V (see the curve "b" for the PPMD diode).

(iii)   Nanoparticles in both the EL and HTL films have contributed to significantly lowering the turn-on voltage of the device (see the curve "c" for the PMCD diode).
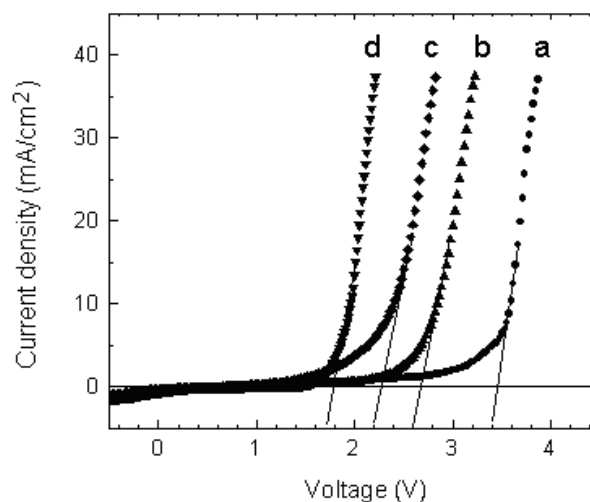

Fig. 15. I-V characteristics of OLED with different laminated structure. (a) – Single MEH-PPV, SMED; (b) – with HTL layer, PPMD; (c) – with HTL and EL composite layers, PMCD and (d) – with LiF, MMCD

The effect of HTL, ETL and/or SCL on the enhancement of the I-V characteristics was well demonstrated, associated with the equalization process of injection rates of holes and electrons. But the reason why the nanoparticles can improve the device performance is still open for discussion. For instance, in (Scott et al., 1996) the authors attributed this enhancement to the stimulated emission of optically-pumped MEH–PPV films when TiO$_2$ particles were embedded in. Whereas, in (Carter et al., 1997) the authors indicated that no evidence of line narrowing or changes in the line shape was observed at different voltages, implying that the mechanism for improved performance was distinctly different from that

found in optically-pumped TiO_2/MEH–PPV films. These latter concluded that optical scattering phenomenon was not causing an enhancement in the device performance. Another possible explanation is that the nanoparticle surfaces increase the probability of electron-hole recombination; however, this would result in a change in the external quantum efficiency, rather than the current density as it was observed.

From the data of PL spectra for the MEH-PPV and the transmittance for PEDOT composites, we have observed both the improvement in PL intensity and the luminescence quenching of the composite (see figure 13 and 14). Similar phenomena obtained for nanohybrid layers were explained due to the TiO_2/polymer boundaries causing a difference in bandgap between the oxide nanoparticles and the conjugate polymer (Thuy et al., 2009). Based on these results, one can advance a hypothesis for the improved performance which supports the suggestion by Carter et al (1997). A change in the device morphology would be caused by the incorporation of nanoparticles into the solution. During the spinning process in the spin-coating technique, the nanoparticles can adhere by strong electrostatic forces to the HTL and between themselves, and capillary forces can then draw the MEH–PPV solution around the nanoparticles into cavities without opening up pinholes through the device. This will result in a rough surface over which the LiF (SCL) is evaporated and subsequently, a large surface area interface between the SCL and the electroluminescent composite material is formed. At a low voltage, charge-injection into MEH–PPV is expected to be cathode limited; the very steep rise in the I–V curves for the composite diodes however suggests that more efficient injection at the cathode through the SCL is occurring which would be caused by the rougher interface of the nanocomposites. At a higher voltage, transport in MEH–PPV appears to be space-charge limited.

The electroluminescence quantum efficiency can be caculated by using a well-known expression:

$$\eta_\phi = \gamma \times \eta_r \times \phi_f \tag{1}$$

where γ is a double charge injection factor which is dependent on the processes of carrier injection and is maximal ($\gamma = 1$) if a balanced charge injection into the emission layer of the device is achieved, i. e. the number of injected negative charges (electrons) equals the number of injected positive charges (holes); η_r quantifies the efficiency of the formation of a singlet exciton from a positive and a negative polaron, and ϕ_f is the photoluminescence quantum efficiency. From the PL spectra and the I-V characteristics obtained one can see that γ for the MMCD is the largest due to the addition of both the HTL and SCL into the device. Since nc-TiO2 particles embedded in MEH-PPV constitute a factor favouring electrons faster move in the EL, the intrinsic resistance of the OLED is lowered. This results in an improvement of the I-V characteristics of the device. Moreover, the more mobile electrons can create a larger probability of the electron-hole pairs formation in the emitting layer, resulting in an increase in ηr for the MMCD. Thus the electroluminescence quantum efficiency of the multilayer polymeric composite diodes can be evaluated from (1) and appears to be much larger than the one for the single polymeric layer device. As a result of the enhanced carriers injection and transport in the polymer composites, the electroluminescence quantum efficiency is roughly estimated to be improved by a factor exceeding about 10.

3. PON composites for inverse OLEDs

3.1. PVK/MoO₃ hybrid structrure

Polypropylene carbazone (PVK) deposited on a nanostructued MoO_3 (PVK/MoO_3), as the PON composite, can be seen as a hybrid structure between a polymer and an inorganic oxide. To prepare a hybrid structure of PVK/nc-MoO_3, Mo metallic substrate was annealed in oxygen, at temperature of 550 °C for ca. 2 hours to get a nanostructured MoO_3 layer, and then PVK was deposited by spin-coating, followed by vacuum annealing. Surface morphology and nano-crystalline structures of MoO_3 were checked, respectively by using Scanning Electron Microscopy (FE-SEM) and X-Rays Diffraction (XRD). I-V characteristics were measured using an Auto-Lab. Potentiostat PGS-30.

The thickness of the annealed Mo substrate layers was found to be dependent of the annealing conditions such as the temperature and time. The samples used for devices were prepared at 500 °C, for 2 hours. The structure of the films was checked by performing X-ray incident beam experiment. For thin annealed layers, three XRD peaks of the Mo substrate are obtained with a strong intensity (denoted by Mo-peaks in figure 15) indicating bulk Mo crystalline structure of the substrate.
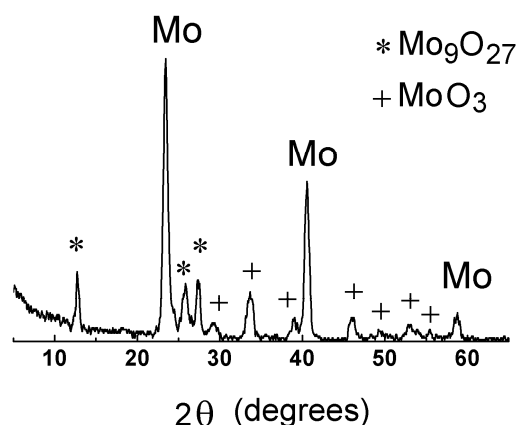

Fig. 15. XRD patterns of an annealed Mo-substrate showing, beside Mo structure, there are two structures of Mo oxides, namely MoO_3 and Mo_9O_{27}

Three other sharp peaks denoted by a star symbol in figure 15 characterize a crystalline structure of Mo_9O_{27} that has been formed upon annealing. In the XRD diagram, there are seven diffraction peaks corresponding MoO_3. The fact that the peak width is rather large shows that the MoO_3 layer was formed by nanocrystalline grains. To obtain the grain size τ we used the Scherrer formula:

$$\tau = \frac{0.9\lambda}{\beta.\cos\theta} \tag{2}$$

where λ is X-ray wavelength, β is the full width at half maximum in radians and θ is the Bragg angle of the considered diffraction peak (Cullity, 1978). The values of β were found from 0.008 to 0.010, consequently the average size of the grains was determined as $\tau \approx 7\text{-}10$ nm. This result is in a good agreement with the data obtained by FE-SEM for the average size of grains. The MoO_3 layer further would be spin-coated by PVK to get a heterojunction of PVK/nc-MoO_3.

Current-voltage characteristics of Ag/Mo/nc-MoO$_3$/PVK/Al and Ag/ITO/PVK/Al (Figure 16) show that the onset voltage of the hybrid junction is lowered in comparison with that of the standard junction. This may be explained by: (i) the workfunction of nc-MoO$_3$ is higher than that of ITO and (ii) the Mo substrate is metallic, thus Ag/Mo contact is more ohmic than Ag/ITO contact.
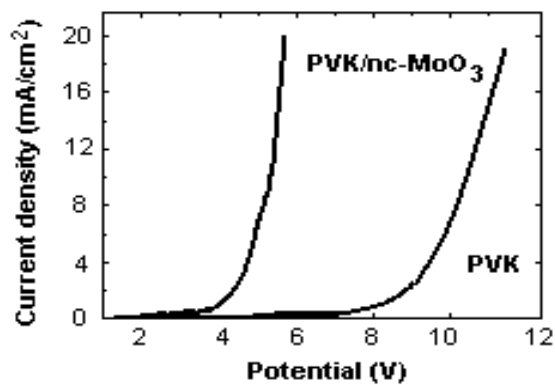

Fig. 16. I-V characteristic of PVK/MoO$_3$/Ag junction (left curve) and PVK/Ag junction (right curve)

3.2. MEH-PPV/TiO$_2$ hybrid structure

As seen in above mentioned PVK/nc-MoO$_3$/Mo hybrid layer, both the photoluminescence and I-V characteristics of the layer have been enhanced in comparison with those of the pure polymer based OLED. Lin et al (2007) showed that when a nanorod-like NIP composite of MEH-PPV+TiO$_2$ was excited by photons of a large energy, its photoluminescence was enhanced in comparison with that of MEH-PPV alone. As far as we know, the photoluminescencent properties of MEH-PPV/nc-TiO$_2$ hybrid PON films have been rarely studied. The aim of our work is to study the photoluminescent behavior of PON hybrid layers, when nanorod-like TiO$_2$ were grown on a flat titanium bar.

To grow nanocrystalline titanium oxide (nc-TiO$_2$) on metallic titanium, a 2-mm thick Ti wafer with a size of 5 mm in width and 10 mm in length were carefully polished using synthetic diamond powder of 0.5μm in size. The polished surface of Ti was ultrasonically cleaned in distilled water, followed by washing in ethylene and acetone. Then the dried Ti wafer was put in a furnace, whose temperature profile could be controlled automatically. We used three different annealing temperature profiles as follows: from room temperature, the furnace was heating up to 700°C for two hours and kept at this temperature respectively for one hour (the first profile), for one and a half hour (the second profile) and for two hours (the third profile), and these processes were followed by a cooling down to room temperature during three hours. To deposit hybrid layers, MEH-PPV solution was prepared by dissolving MEH-PPV powder (product of Aldrich, USA) in xylene with a proportion of 10 mg of MEH-PPV in 1 ml of xylene. The spincoating was carried-out in gaseous nitrogen with a set-up procedure described in the following. The delay time was 120s, the rest spin time 30s, the spin speed 1500 rpmin, the acceleration 500 rpmin and the relaxation time 5 min. After spincoating the samples were put into a vacuum oven for drying at 120°C at 1.33 Pa for 2 hours. For I-V testing, a silver-aluminum alloy coating

was evaporated on the polymer to make diodes with the structure of AgAl/MEH-PPV/nc-TiO_2/Ti (Thuy et. al, 2009).

3.2.1 Morphology and crystalline structure of nanoporous TiO2 layer

Samples which were annealed respectively according to the first, second and third temperature profile are referred to by TC1, TC2 and TC3. The hybrid films having a structure of MEH-PPV/Ti-substrate, MEH-PPV/TC1, MEH-PPV/TC2 and MEH-PPV/TC3 are respectively abbreviated to MEHPPV, PON1, PON2 and PON3 for photoluminescence measurements. Similar symbols are adopted for the heterojunctions samples used in I-V tests, as follows:

MEHPPV: Ag-Al/MEH-PPV/Ti-substrate/Ag
PON1: Ag-Al/PON1/Ti-substrate/Ag
PON2: Ag-Al/PON2/Ti-substrate/Ag
PON3: Ag-Al/PON3/Ti-substrate/Ag

Figure 17 shows the FE-SEM images of three samples (TC1, TC2 and TC3). For all the samples TiO_2 was grown in form of nanorods whose size was strongly dependent on conditions of the thermal treatment. These pictures reflect a very high resolution of the FE-SEM: one can determine approximately both the size on the surface and the depth (or length) of TiO_2 rods grown in the titanium wafer. Thus, TiO_2 rods in TC2 (annealing time is 1.5 h) were estimated to have a width of about 70 nm on average and a length of about 200 nm. Moreover, a large number of the rods have orientation close to the vertical direction (see figure 17b). For the TC1 (Figure 17a) and TC3 (Figure 17c) samples, TiO2 rods were randomly orientated, TCl being thinner than TC3. The annealing time of TC3 was larger than that of TC2, and TC1, TC2 and TC3 had thicknesses respectively equal to ca. 100, 200 and 150 nm. We also annealed Ti wafers at the temperature of 500°C or 800°C. Even with a different annealing process, pictures of the nanorods on titanium substrate were similar to those for TC1 and TC3. This shows that for growing a nanorod-like TiO_2 on titanium surfaces, the temperature can be maintained at 700°C for 1.5 h.

Figure 18 shows XRD patterns of TC1 (top), TC2 (middle) and TC3 (bottom) samples. Although the annealed layers of the samples are thin (i.e. ~ 200 nm), in the XRD patterns all the key characteristic peaks of a rutile TiO_2 crystal are revealed. These peaks correspond to space distances of 0.322, 0.290, 0.217, 0.205, 0.168, 0.162 and 0.115 nm for all the samples. The fact that two intensive peaks of the titanium crystal (0.245 and 0.224 nm) occurred proves that X-ray went through the TiO_2 layer and interacted with the titanium crystalline lattice. Using formula (2) for the determination of crystalline grain size of the TiO_2, an average value calculated for all the TiO_2 peaks was found to be around 100 nm for the TC2 sample. This value is fairly different for TC1 and TC3 samples. However, these results are in a good agreement with the results by FE-SEM.
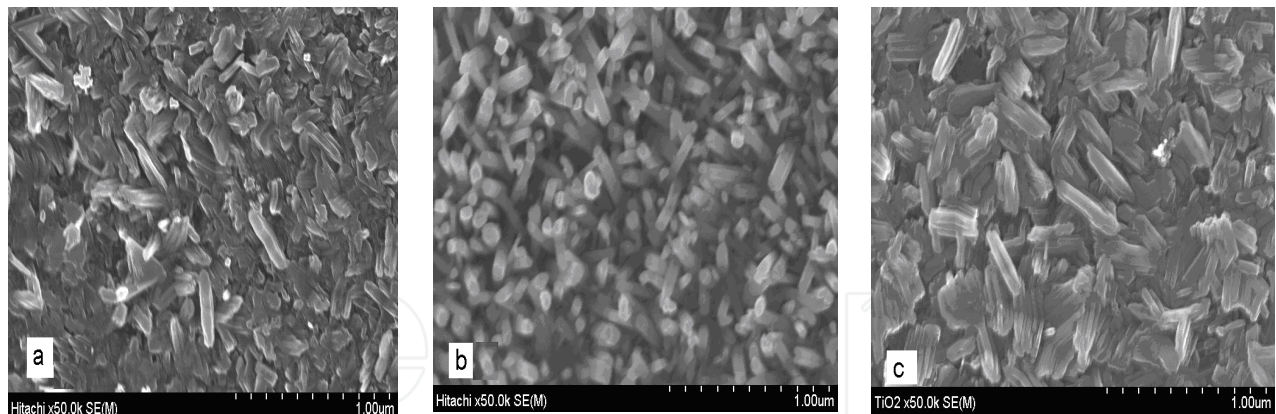
Fig. 17. FE-SEM pictures of annealed titanium surfaces: (a) 700 ᵒC for 1 h (TC1), (b) 700°C for 1.5 h (TC2) and (c) 700°C for 2 h (TC3). The thickness of nc-TiO$_2$ layers is of 100 nm, 200 nm and 150 nm, respectively for TC1, TC2 and TC3 samples
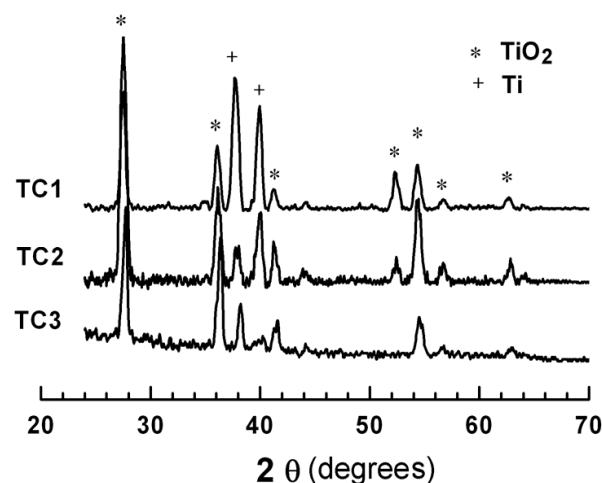

Fig. 18. XRD patterns of nc-TiO$_2$ layers grown on Ti surfaces at 700ᵒC for 1h (TC1), 1.5h (TC2) and 2h (TC3)

3.2.2 Photoluminescent and electrical properties of hybrid junctions

The results of PL measurements of all the samples excited at a short wavelength (ca. 325nm) and at a standard one (ca. 470 nm) are presented. Figure 19 shows plots of the PL spectra measured on MEH-PPV, PON1, PON2 and PON3 samples, using the FL3-2 spectrophotometer with an He-Ne laser as an excitation source (λ = 325 nm). It is seen that all the samples have broad photoemission at two peaks; one higher at 645 nm and another lower at 605 nm. In a work on MEH-PPV+nc-TiO$_2$ composite (Carter et al., 1997) the author reported that two electroluminescence peaks at 580 nm and 640 nm occurred, where the first peak was higher than the second one. This negligible difference in wavelength values and intensity of the emission peaks can be explained due to electroluminescence. The emission peaks are shifted to longer wavelengths with respect to the main absorbance band. This red-shift is explained due to emission of the most extensively conjugated segments of the polymer (Kersting et al., 1993). From figure 19, it is seen that photoemission of all the hybrid samples exhibit higher luminescence intensity than that of the pure MEH-PPV. However, PL strongest enhancement occurred in PON2 film while for PON1 and PON3 films PL the intensities were not much increased. In these hybrid films no blue shift was

observed, as it was obtained for MEH-PPV + nc- TiO_2 (see figure 13) or for PPV+nc-SiO_2, (Yang et al., 2005), as NIP composites. The blue shift was explained by the reduction of the polymer conjugation chain length. Although PL enhancement has been rarely mentioned, one can suggest that the increase PL intensity for such a PON2 thin film can be explained by the large absorption coefficient for TiO_2 nanorods. This similar the effect observed for the MEHPPV-NIP films, which explained due to the non-radiative Förster resonant energy transfer (Heliotis et. al., 2006) from TiO_2 nanorods to polymer with excitation of wavelength less 350 nm.
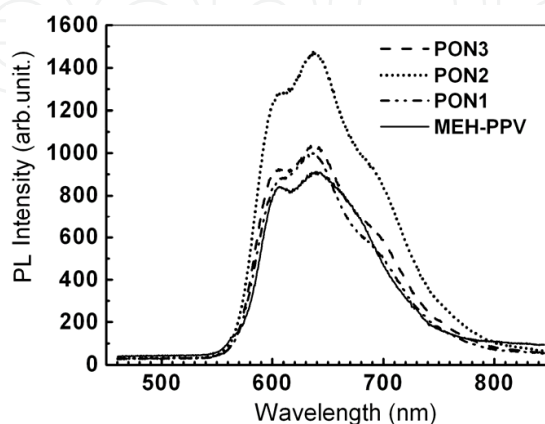
Fig. 19. PL spectra of MEH-PPV and nanohybrid films by using a He-Ne laser excitation at 325 nm. The best PL enhacement is obtained for PON2 sample

In Figure 20 the PL spectra of MEH-PPV and hybrid film samples with excitation wavelength of 470 nm (on FL3-22 using Xe lamp) are plotted. In this case, the MEH-PPV luminescence quenching occurred clearest in the PON2 sample. These spectra exhibited quite similarly to the spectra obtained for the MEH-PPV+nc-TiO_2 (NIP) samples (see figure 14).
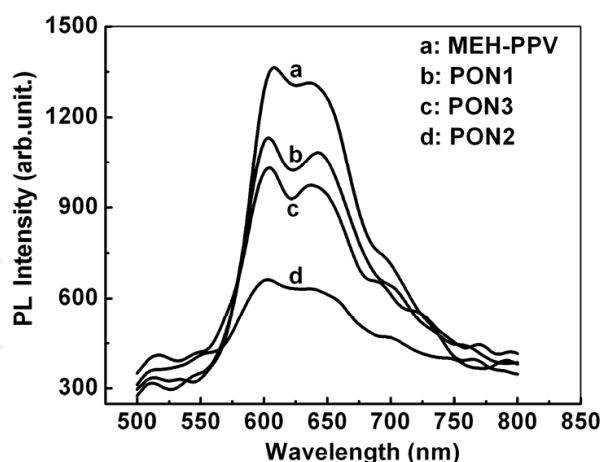

Fig. 20. PL spectra of MEH-PPV and nanohybrid films by using a Xe lamp excitation at 470 nm. The strongest MEH-PPV fluorescence quenching is obtained for PON2 sample

For all the samples the photoemission has two broad peaks at 605 nm and 645 nm as in the case of short wavelength excitation. Moreover, from figure 19 and figure 20 one can see that in these samples the larger enhancement in PL intensity (under short wavelength excitation), the stronger fluorescence quenching (under normal excitation) has occurred. The fact that the peak at 605 nm is larger than the peak at 645 nm is similar to the

electroluminescence spectra plotted in a work of Carter et al (1997). As seen in a work of Petrella et al (2004), for a NIP composite, in presence of rod-like TiO_2 nanocrystals, PPV quenching of fluorescence is significantly high. This phenomenon has been explained due to the transfer of the photogenerated electrons to the TiO_2. In our case, among three hybrids films the PON2 sample is the most porous, and the rods are well separated from each other. Thus this sample is likely to be a NIP composite. Perhaps, this is the reason why PON2 exhibited the strongest quenching effect.

3.2.3 Current-voltage characteristics

Figure 21 shows the I-V curves of a pure MEH-PPV based diode and three hybrid diodes denoted as PON1, PON2 and PON3. It is seen that such a diode of Ag/Ti/MEHPPV/AlAg does not have both the transparent anode and hole transport layer (HTL). Thus, stating from some applied voltage, IV characteristics present a linear dependence of current on voltage as for a resistance (bottom curve, figure 5). For all the nanohybrid devices a turn-on voltage is of around 3 V, ascending from PON2 sample to PON1 and PON3, but the current density is not large (about $5 \div 10$ mA/cm^2 at 4 V). For PON2 device although the turn-on voltage is smaller, the current began increasing with voltage right from 0. For PON1 and PON3 devices, it grew up from 2 V. This means that in the PON2 the reverse current of the device appeared from starting switch-on voltage, it can cause the device to be heated up. The PON1 and PON3 devices have a rather low turn-on voltage and no reverse current was observed up to an applied voltage of 2 V. It is known (Carter et al., 1997) that the fluorescence quenching of MEH-PPV results in charge-separation at interfaces of TiO_2/MEH-PPV, consequently reducing the barrier height at the last. This indicates that the PON2 film will be a better candidate for a photovoltaic solar cell than for the OLED.
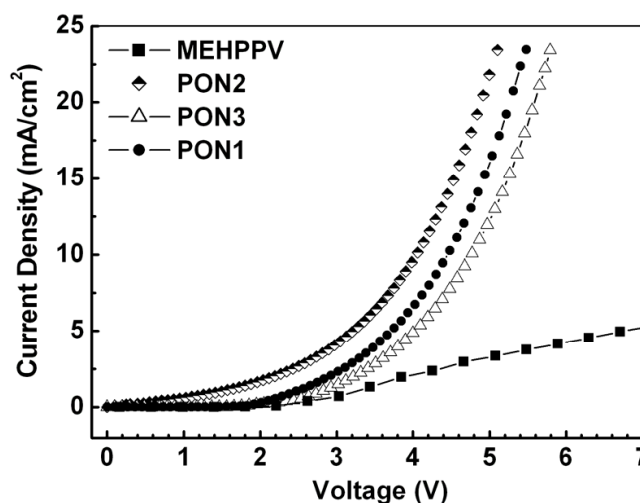

Fig. 21. I-V characteristics measurement of AgTi/MEH-PPV/Al-Ag (MEHPPV) and three devices of Ag/Ti/MEH-PPV+nc-TiO_2/Al-Ag (PON1, PON2 and PON3)

The fact, that PON1 and PON3 samples have very weak fluorescence quenching means that under the light illumination an inconsiderable electron/hole generation may occur at the TiO_2/MEH-PPV interfaces. Therefore, the PON1 and PON3 are not suitable for the photocurrent conversion. However, the improvement in I-V of the PON1 and PON3 devices can be attributed to a thin TiO_2 layer sandwiched between the polymer and Ti substrate. In

this case the nc-TiO$_2$ layer played the role of HTL in OLEDs. Thus, contrarily to the PON2, such a laminar device as Ag-Al/PON/Ti/Ag is preferable to be used for OLEDs rather than for polymeric solar cells. However, to make a reverse OLED, instead of AgAl thin film, it is necessary to deposit a transparent cathode onto the emitting layer.

4. Conclusion and remarks

We have given an overview of the recent works on nanocomposites used for optoelectronic devices. From the review it is seen that a very rich publication has been issued regarding the nanostructured composites and nano-hybrid layers or heterojunctions which can be applied for different practical purposes. Among them there are organic light emitting diodes (OLED) and excitonic or organic solar cells (OSC).

Our recent achievements on the use of nanocomposites for OLEDs were also presented. There are two types of the nanocomposite materials, such as nanostructured composites with a structure of nanoparticles embedded in polymers (abbreviated to NIP) and nanocomposites with a structure of polymers deposited on nanoporous thin films (called as PON). Embedding TiO$_2$ nanoparticles in PEDOT, one can obtain the enhancement of both the contact of hole transport layer with ITO and the working function of PEDOT films. The improvement was attributed to the enhancement of the hole current intensity flowing through the devices. The influence of nanooxides on the photoelectric properties of the NIPs is explained with regard to the fact that TiO$_2$ particles usually form a type-II heterojunction with a polymer matrix, which essentially results in the separation of nonequilibrium electrons and holes. NIPs with the TiO$_2$ nanoparticles in MEH-PPV have been studied as photoactive material. MEH-PPV luminescence quenching is strongly dependent on the nature of nanostructral particles embedded in polymer matrix. Actually, the higher quenching of the polymer fluorescence observed in presence of titania nanoparticles proves that transfer of the photogenerated electrons to TiO$_2$ is more efficient for rods. Characterization of the nanocomposite films showed that both the current-voltage (I-V) characteristics and the photoluminescent properties of the NIP nanocomposite materials were significantly enhanced in comparison with the standard polymers. OLEDs made from these layers can exhibit a large photonic efficiency. For a PON-like hybrid layer of MEH-PPV/nc-TiO$_2$, the photoluminescence enhancement has also been observed. Thin nanostructured TiO$_2$ layers were grown by thermal annealing, then they were spin-coated by MEH-PPV films. Study of PL spectra of pure MEH-PPV and MEHPPV-PON films has shown that with excitation by a 331.1 nm wavelength laser lead to the largest enhancement in photoluminescent intensity as observed in the PON samples, and with an excitation of a 470 nm wavelength laser, the strongest fluorescence quenching occurred in this sample too. Current-voltage characteristics of laminar layer devices with a structure of Ti/PON/Al-Ag in comparison with that of Ti/MEH-PPV/Al-Ag showed that the turn-on voltage of the devices was lowered considerably. Combining I-V with SEM and PL, it is seen that PON are suitable for an reverse OLED, where the light goes out through the transparent or semi-transparent cathode, moreover to do Ohmic contact to the metallic Ti electrode is much easier.

However, to realize making reverse OLEDs, it is necessary to carry-out both the theoretical and technological researches to find out appropriate materials which can be used for the transparent cathode.

5. References

Burlakov, V. M.; Kawata, K.; Assender, H. E.; Briggs, G. A. D.; Ruseckas, A. & Samuel, I. D. W. (2005). Discrete hopping model of exciton transport in disordered media. *Physical Review* 72, pp. 075206-1 ÷ 075206-5.

Carter, S. A.; Scott, J. C. & Brock, J. (1997). Enhanced luminance in polymer composite light emitting diodes. *J. Appl. Phys.* **71(9)**, pp. 1145 – 1147.

Cullity, B. D. (1978). *Elements of X-Ray diffraction*, 2nd ed., p.102. Addison, Wesley Publishing Company, Inc., Reading, MA.

Dinh, N. N.; Chi L. H., Thuy, T.T.C; Trung T.Q. & Vo, Van Truong. (2009). Enhancement of current, voltage characteristics of multilayer organic light emitting diodes by using nanostructured composite films, *J. Appl. Phys.* 105, pp. 093518-1÷ 093518-7.

Dinh, N. N.; Chi, L. H.; Thuy, T. T. C.; Thanh, D. V. & Nguyen, T. P. (2008). Study of nanostructured polymeric composites and hybrid layers used for Light Emitting Diodes. *J. Korean Phys. Soc.* **53**, pp. 802-805.

Dinh, N. N.; Trung, T. Q.; Le H. M.; Long P. D. & Nguyen T., P. (2003). Multiplayer Organic Light Emmiting Diodes: Thin films preparation and Device characterization, *Communications in Physics* 13, pp. 165-170.

Dittmer, J. J.; Marseglia, E. A. & Friend, R. H. (2000). Electron Trapping in Dye/Polymer Blend Photovoltaic Cells. *Adv. Mater.* 12, pp.1270-1274.

Haugeneder, A.; Neges, M.; Kallinger, C.; Spirkl, W.; Lemmer, U. & Felmann, J. (1999). Exciton diffusion and dissociation in conjugated polymer/fullerene blends and heterostructures. *Phys. Rev. B, 59*, pp. 15346–15351.

Heliotis, G.; Itskos, G.; Murray, R.; Dawson, M. D.; Watson, I. M & Bradley, D. D. C. (2006). Hybrid inorganic/organic semiconductor heterostructures with efficient non, radiative Förster energy transfer. *Adv. Mater.* **18**, pp. 334-341.

Huynh, W. U.; Dittmer, J. J. & Alivisatos, A. P. (2002). Hybrid Nanorod, Polymer Solar Cells. *Science* 295, pp. 2425 – 2427.

Kersting, R.; Lemmer, U.; Marht, R. F.; Leo, K.; Kurz, H.; Bassler, H. & Gobel, E. O. (1993). Femtosecond energy relaxation in π, conjugated polymers. *Phys. Rev. Lett.* **70**, pp. 3820 – 3823.

Klabunde, K. J. (2001). *Nanoscale Materials in Chemistry*, John Wiley & Sons.

Lin, Yu, Ting.; Zeng, Tsung, Wei.; Lai, Wei, Zong.; Chen, Chun, Wei.; Lin, Yun, Yue.; Chang, Yu, Sheng. & Su, Wei, Fang. (2006). Efficient photoinduced charge transfer in TiO_2 nanorod/conjugated polymer hybrid materials. *Nanotechnology* 17, pp. 5781–5785.

Ma, W.; Yang, C.; Gong, X.; Lee, K. & Heeger, A. J. (2005). Thermally Stable, Efficient Polymer Solar Cells with Nanoscale Control of the Interpenetrating Network Morphology. *Adv. Func. Mater.* 15, pp.1617 – 1622.

Petrella, T. M.; Cozzoli, P. D.; Curri, M. L.; Striccoli, M.; Cosma, P.; Farinola, G. M.; Babudri, F.; Naso, F. & Agostiano, A. (2004). TiO_2 nanocrystals – MEH, PPV composite thin films as photoactive material. *Thin Solid Films* 451/452, pp. 64–68.

Quyang, J.; Chu, C., W.; Chen, F., C.; Xu, Q. & Yang, Y. (2005). High, Conductivity Poly(3,4, ethylenedioxythiophene): Poly(styrene sulfonate) Film and Its Application in Polymer Optoelectronic Devices. *Advanced Functional Materials* **15,** pp. 203 - 208.

Quyang, J.; Xu, Q.; Chu, C., W.; Yang, Y.; Li, G. & Shinar, J. (2004). On the mechanism of conductivity enhancement in poly(3,4, ethylenedioxythiophene):poly(styrene sufonate) film through solvent treatment. *Polymer* **45**, pp. 8443 - 8450.

Ravirajan, P.; Bradley, D. D. C.; Nelson, J.; Haque, S. A.; Durrant, J. R.; Smit, H. J. P. & Kroon, J. M. (2005). Efficient charge collection in hybrid polymer/TiO_2 solar cells using poly(ethylenedioxythiophene)/polystyrene sulphonate as hole collector. *Appl. Phys. Lett.* 86, pp. 143101 - 143113.

Salafsky, J. S. (1999). Exciton dissociation, charge transport, and recombination in ultrathin, conjugated polymer, TiO2 nanocrystal intermixed composites. *Physical Review B* 59, pp. 10885 – 10894.

Scott, J. C.; Kaufman, J.; Brock, P. J.; DiPietro, R.; Salem, J. & Goitia, J. A. (1996). MEH, PPV Light, Emitting Diodes: Mechanisms of Failure. *J. Appl. Phys.* 79, pp. 2745 – 2753.

Tehrani, P.; Kanciurzewska, A.; Crispin, X.; Robinson, N. D.; Fahlman, M. & Berggren, M. (2007). The effect of pH on the electrochemical over, oxidation in PEDOT:PSS films. *Solid State Ionics* 177, pp. 3521 – 3528.

Thuy, T. T.C.; Chi, L. H. & Dinh, N. N. (2009). Study of Photoluminescent and Electrical Properties of Nanostructured MEH, PPV/ TiO_2 hybrid films, *JKPS* 54, pp. 291 - 295.

Yang, S. H.; Nguyen, T. P.; Le Rendu, P. & Hsu, C. S. (2005). Optical and electrical properties of PPV/SiO_2 and PPV/TiO_2 composite materials. *Composites Part A: Appl. Sci..Manufact.* 36, pp. 509 - 513.
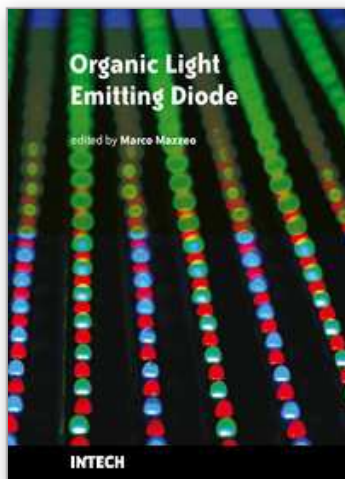
Organic Light Emitting Diode

Edited by Marco Mazzeo

ISBN 978-953-307-140-4

Hard cover, 224 pages

Publisher Sciyo

Published online 18, August, 2010

Published in print edition August, 2010

Organic light emitting diodes (OLEDs) have attracted enormous attention in the recent years because of their potential for flat panel displays and solid state lighting. This potential lies in the amazing flexibility offered by the synthesis of new organic compounds and by low-cost fabrication techniques, making these devices very promising for the market. The idea that flexible devices will replace standard objects such as television screens and lighting sources opens, indeed, a new scenario, where the research is very exciting and multidisciplinary. The aim of the present book is to give a comprehensive and up-to-date collection of contributions from leading experts in OLEDs. The subjects cover fields ranging from molecular and nanomaterials, used to increase the efficiency of the devices, to new technological perspectives in the realization of structures for high contrast organic displays and low-cost organic white light sources. The volume therefore presents a wide survey on the status and relevant trends in OLEDs research, thus being of interest to anyone active in this field. In addition, the present volume could also be used as a state-of-the-art introduction for young scientists.

INTECH
open science | open minds